

Charge transfer and asymmetric coupling of MoSe₂ valleys to the magnetic order of CrSBr

C. Serati de Brito,^{†,‡} P. E. Faria Junior,[¶] T. S. Ghiasi,[§] J. Ingla-Aynés,[§] C. R. Rabahi,[†] C. Cavalini,[†] F. Dirnberger,^{||} S. Mañas-Valero,^{§,⊥} K. Watanabe,[#] T. Taniguchi,[#] K. Zollner,[¶] J. Fabian,[¶] C. Schüller,[‡] H. S. J. van der Zant,[§] and Y. Galvão Gobato^{*,†}

[†]*Physics Department, Federal University of São Carlos, São Carlos, SP, 13565-905, Brazil*

[‡]*Institut für Experimentelle und Angewandte Physik, Universität Regensburg, D-93040 Regensburg, Germany*

[¶]*Institute of Theoretical Physics, University of Regensburg, 93040 Regensburg, Germany*

[§]*Kavli Institute of Nanoscience, Delft University of Technology, Lorentzweg 1, 2628 CJ Delft, The Netherlands*

^{||}*Institute of Applied Physics and Würzburg-Dresden Cluster of Excellence ct.qmat, Technische Universität Dresden, Germany*

[⊥]*Instituto de Ciencia Molecular (ICMol), Universitat de València, Catedrático José Beltrán 2, Paterna 46980, Spain*

[#]*Research Center for Materials Nanoarchitectonics, National Institute for Materials Science, 1-1 Namiki, Tsukuba 305-0044, Japan*

E-mail: yara@df.ufscar.br

Abstract

Van der Waals (vdW) heterostructures composed of two-dimensional (2D) transition metal dichalcogenides (TMD) and vdW magnetic materials offer an intriguing platform to functionalize valley and excitonic properties in non-magnetic TMDs. Here, we report magneto-photoluminescence (PL) investigations of monolayer (ML) MoSe₂ on the layered A-type antiferromagnetic (AFM) semiconductor CrSBr under different magnetic field orientations. Our results reveal a clear influence of the CrSBr magnetic order on the optical properties of MoSe₂, such as an anomalous linear-polarization dependence, changes of the exciton/trion energies, a magnetic-field dependence of the PL intensities, and a valley g -factor with signatures of an asymmetric magnetic proximity interaction. Furthermore, first principles

calculations suggest that MoSe₂/CrSBr forms a broken-gap (type-III) band alignment, facilitating charge transfer processes. The work establishes that antiferromagnetic-nonmagnetic interfaces can be used to control the valley and excitonic properties of TMDs, relevant for the development of opto-spintronics devices.

Keywords

Transition Metal Dichalcogenides, two-dimensional magnets, van der Waals Heterostructures, Proximity Effects, Magneto-Optics.

Recently, van der Waals (vdW) magnetic materials have attracted increasing attention be-

cause of their unique magnetic properties and possible applications in spintronics.¹⁻¹³ Several studies were performed in heterostructures using magnetic materials and monolayer TMDs.^{1-3,14-22} These heterostructures employ magnetic proximity effects to modify the physical properties of the ML TMD adjacent to the magnetic material and therefore offer new opportunities for engineering magnetic heterostructures.¹⁸ Actually, recent studies evidenced an enhanced valley splitting of WSe₂ and WS₂ monolayers on the ferromagnetic (FM) material EuS,^{23,24} a giant zero-field valley splitting of MoSe₂/CrBr₃,²⁵ asymmetric magnetic proximity interactions in MoSe₂/CrBr₃,¹⁶ and an anomalous temperature dependence of the MoSe₂/MnPSe₃ excitonic peak below the Néel temperature (T_N).³ Furthermore, magnetic proximity effects have led to spin-dependent charge transfer and concomitant circularly polarized PL in hybrid devices based on both CrI₃^{2,17} and CrBr₃.¹ However, most previous studies in magnetic vdW heterointerfaces involved vdW ferromagnetic materials.¹⁻⁶ AFM materials have a variety of spin orderings with distinct magnetic symmetry groups which could result in unique magnetic properties and therefore there are interesting ways to control their functionalities by choosing appropriate AFM materials.³

In this work, we investigate the impact of the CrSBr antiferromagnetic substrate on the exciton and valley properties of ML MoSe₂. We have performed micro-PL measurements under a magnetic field along each of the three crystallographic axes of CrSBr. In general, our findings show that the exciton and valley properties of ML TMDs can be engineered by the interplay of magnetic proximity, efficient charge transfer effects, exciton/trion-magnon coupling and dielectric anomalies of 2D antiferromagnetic materials.

The layered magnetic material CrSBr is a vdW direct gap semiconductor with A-type AFM and Néel temperature of 132 K in its bulk form.²⁶⁻³⁴ In addition, CrSBr presents another phase transition around the temperature of $T = 40$ K^{7,29,30} which is not well understood but might be related to crystal defects²⁶ or

spin-freezing effects.¹³ The CrSBr crystal consists of layers with rectangular unit cells in the plane ($\hat{a} - \hat{b}$) which are stacked along the \hat{c} axis to produce an orthorhombic structure [Figure 1(b)]. The optical properties of CrSBr reflect its highly anisotropic electronic and magnetic structure. A prominent example is the coupling of excitons to the magnetic order. Changes in the static magnetic configuration induced by applying a magnetic field, for instance, directly impact the exciton energy. The electronic band structure, and consequently the energy of excitons in CrSBr, are sensitive to the interlayer magnetic exchange interaction which can be used to probe its magnetic properties.^{7,28,30,34}

Monolayer MoSe₂ is a direct band gap semiconductor with two inequivalent $\pm K$ valleys and robust excitons.³⁵⁻⁴³ Under out-of-plane magnetic fields, valley Zeeman effects and magnetic-field-induced valley polarization are observed and these effects depend on the presence of strain, doping and magnetic proximity effects.^{25,44-56}

Figure 1 (a) shows an optical microscope image of our MoSe₂/CrSBr heterostructure and the crystal orientations, \hat{a} and \hat{b} , of the CrSBr bulk crystal, while in Figure 1 (b) the MoSe₂ and CrSBr crystal structures are sketched. Figure 1 (c) presents the predicted type-III (broken-gap) band alignment of the heterostructure. In Figure 1 (d), the PL spectrum of CrSBr at 3.6 K is displayed in the left part. Several PL peaks are observed below 1.4 eV and associated with excitons,^{7,34,57,58} defects,²⁶ and strong exciton-photon coupling.⁵⁹

Figure 1 (d) shows the exciton and trion peaks in the normalized PL spectra of MoSe₂/CrSBr and MoSe₂/SiO₂. According to our theoretical predictions for the band alignment [see Figures 2 (e-f)], the MoSe₂ layer may be strongly p-doped, while MoSe₂ on SiO₂ is usually n-doped.^{47,52} Therefore, the trion in MoSe₂/CrSBr is most likely a positively charged exciton. In addition, a low-energy shoulder in the trion emission is observed which could be due to inelastic scattering of trions by magnons, or due to localized trions at charged impurities.⁶⁰

Next, we investigate the light-polarization

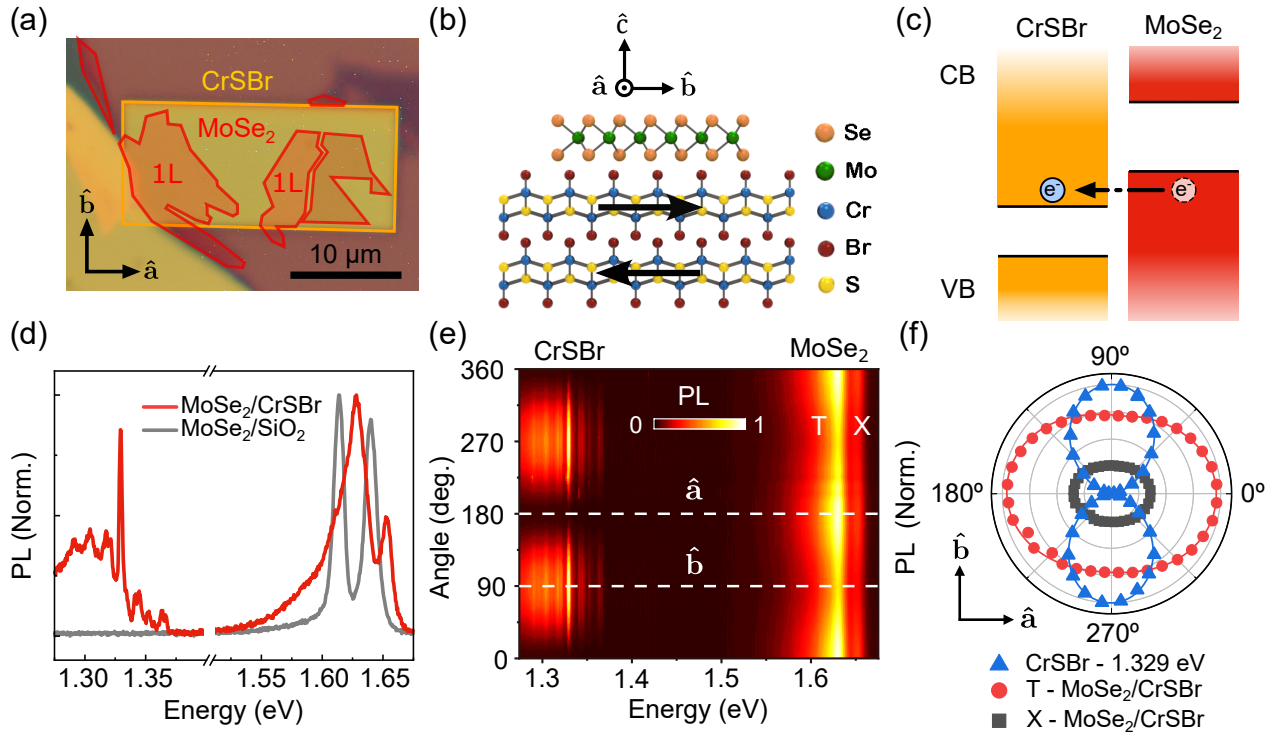


Figure 1: (a) Optical microscope image of the studied ML MoSe₂/bulk CrSBr vdW heterostructure, covered with a thin layer of hBN. The thickness of our CrSBr layer is about 35 nm (Figure S1) (b) Schematics of the crystal structure of the heterostructure. (c) Schematics of the band alignment of ML MoSe₂/bulk CrSBr and charge transfer from the MoSe₂ valence band (VB) to the CrSBr conduction band (CB). (d) Typical PL spectra from ML MoSe₂/CrSBr and MoSe₂/SiO₂ regions at 3.6 K. The laser energy is 1.88 eV. (e) Color-coded map of the linearly-polarized emission intensity as a function of the angle of in-plane polarization. The laser excitation is linearly polarized along the \hat{a} axis (f) Polar plot of the PL intensity versus the in-plane linear polarization angle for the most intense PL peak energy of CrSBr (1.329 eV) and also for the exciton (X) and trion (T) emission peaks from MoSe₂ on CrSBr.

properties in detail. The anisotropic optical emission of the CrSBr layer is evidenced by linear-polarization-resolved PL measurements. Figure 1 (e) shows a color map of the linearly-polarized PL intensity as a function of the in-plane linear polarization angle at 3.6 K. The polar plots for these emissions are shown in Figure 1 (f). All CrSBr PL peaks are strongly linearly polarized along the \hat{b} axis, which evidences the anisotropic electronic structure of CrSBr, as expected. Remarkably, a clear dependence of the PL intensity on the in-plane polarization angle is observed for both, the MoSe₂ exciton [black squares in Fig. 1 (f)] and trion [red circles in Fig. 1 (f)] emissions. This result indicates that the MoSe₂ has acquired a linear-polarization component along the \hat{a} axis

probably due to magnetic proximity or photonic effects due to the linear dichroism of CrSBr.

We have also measured the PL for different magnetic field (\vec{B}) orientations. Figures 2 (a) and (c) show color maps of the MoSe₂/CrSBr magneto-PL intensity under \vec{B} parallel to the in-plane easy ($\vec{B} \parallel \hat{b}$) and hard axis ($\vec{B} \parallel \hat{a}$), respectively. For $\vec{B} \parallel \hat{b}$, the PL spectrum of CrSBr red-shifts abruptly by about 15 meV above a field of 0.375 T and is constant above 0.375 T (see also Figures S6 and S7). This result is similar to previous magneto-optical measurements for few-layer CrSBr²⁸ and was explained by a spin-flip transition from AFM to FM order also observed in magnetization measurements.²⁶ Under $\vec{B} \parallel \hat{a}$, the PL spectrum shifts smoothly, due to the canting of

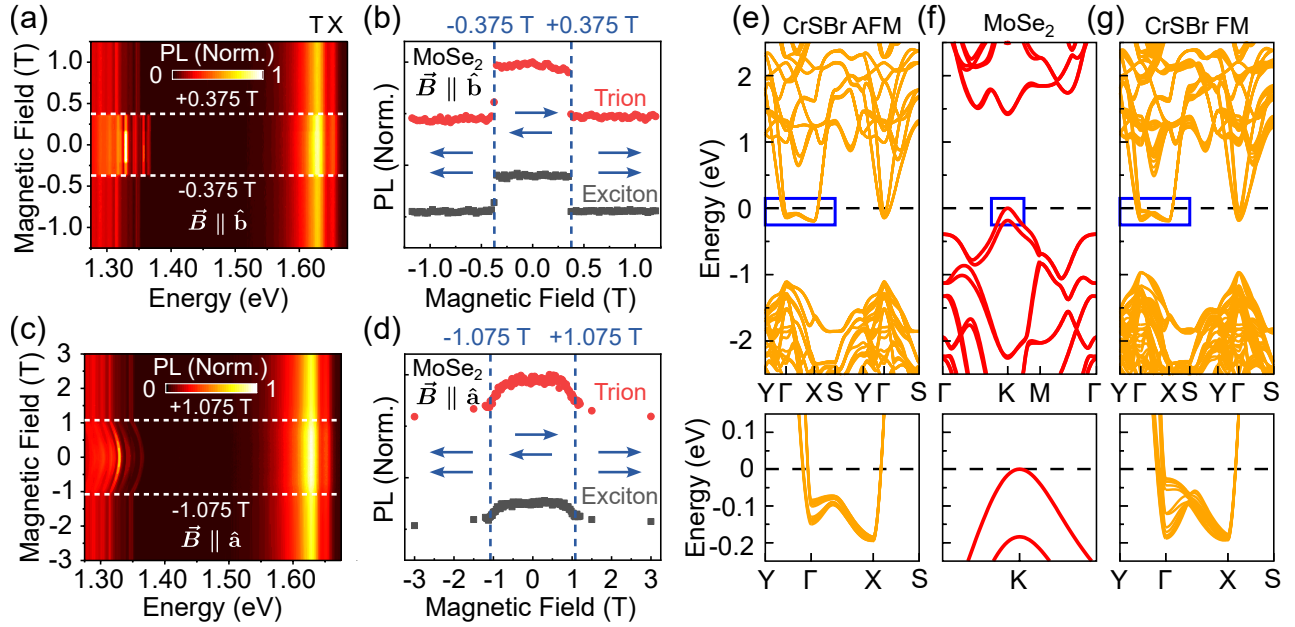


Figure 2: (a,c) Color-code map for circularly-polarized PL intensity from the MoSe₂/CrSBr heterostructure as a function of the in-plane magnetic field, oriented along the in-plane easy (for $\vec{B} \parallel \hat{b}$) and intermediate axes (for $\vec{B} \parallel \hat{a}$). The excitation is performed using a linearly polarized laser. The PL detection is σ^- for positive magnetic fields. (b,d) Magnetic-field dependence of the MoSe₂ PL intensity of the exciton and trion emissions for both field orientations; the MoSe₂ PL intensity is sensitive to the magnetic phases of the CrSBr. Calculated band structure with spin-orbit coupling for (e) CrSBr AFM, (f) ML MoSe₂, and (g) CrSBr FM systems. The CrSBr systems consist of 6 layers. The horizontal dashed lines indicate the Fermi energy aligned with respect to the vacuum levels. The bottom panels show the band structure in the region of the blue rectangles, indicating clear differences of the AFM and FM energy levels next to the Fermi energy.

the spins along \vec{B} , saturating at $B = 1.075$ T beyond which the PL spectrum remains unchanged. The observed PL red shifts of CrSBr with increasing magnetic field was explained by a magnetization-dependent interlayer electronic coupling in the CrSBr material.²⁸

Remarkably, we also find that the PL intensities of the MoSe₂ trion and exciton are correlated to the field-induced phase transition in CrSBr bulk: for $\vec{B} \parallel \hat{b}$ an abrupt change of the PL intensity of MoSe₂ above the critical magnetic field of 0.375 T occurs [see Figure 2 (b) and Figures S6 and S7], and for $\vec{B} \parallel \hat{a}$, a continuous decrease of both MoSe₂ PL intensities is present up to 1.075 T, which corresponds to the saturation of the magnetization in CrSBr. Furthermore, the relative intensity of the trion/exciton peaks (Figure S8) also shows an abrupt change for $\vec{B} \parallel \hat{b}$, above the critical field 0.375 T, and a continuous change up to

1.075 T for $\vec{B} \parallel \hat{a}$, which would indicate an increase in the doping of MoSe₂. This could be explained by a change of charge transfer after the magnetic-field-induced phase transition.

These results can be rationalized by our first principles calculations of the electronic band structure shown in Figures 2 (e-g). Not only the electronic structures of CrSBr in the AFM/FM phases are different^{28,61} but also their band alignment (type-III) with respect to MoSe₂ changes [see bottom panels in Figures 2 (e-g)]. These energetic differences suggest that the charge transfer between ML MoSe₂ and CrSBr can be drastically altered when increasing the magnetic field because of the transition from AFM to FM phases in CrSBr.

Let us now turn to the magneto-PL investigations of the MoSe₂/CrSBr heterostructure for an out-of-plane magnetic field ($\vec{B} \parallel \hat{c}$) under linearly-polarized excitation and σ^- circularly-

polarized PL detection as a function of \vec{B} . For CrSBr emission energies [Figure 3 (a)], a continuous red-shift of all PL peaks occurs while increasing B (in absolute value) up to a saturation field of about 2.25 T, beyond which the PL peaks remains unchanged, consistent with previous reports.²⁸ For MoSe₂, the color code map of PL intensity as a function of B is shown in Figure 3 (b). It also exhibits a correlation with the magnetic phase order of CrSBr. Figure 3 (c) presents the intensities of the exciton and trion PL peaks as a function of the B . We observe an unusual change of the PL intensity for both, exciton and trion, in the range of -2.25 to +2.25 T, which is correlated to the magnetic-field-induced phase transition of CrSBr. In addition, we observe a blue (red) shift of PL peak positions as shown in Figure 3 (b) and (d) with an increase of positive (negative) B values, resembling the effects of the valley Zeeman splitting.^{47,48}

The B dependence for one particular polarization branch (σ^+ or σ^-) of the PL peak of the exciton or trion in TMDs can be written as^{50,62,63}

$$E_i(B) = E_i(B = 0) + g_i^j \mu_B B, \quad (1)$$

in which μ_B is the Bohr magneton, the subindex $i = X$ (T) identifies the exciton (trion), and the superindex $j = \pm$ denotes the circular polarization σ^\pm . Equation (1) describes the Zeeman shift of one polarization branch (the increase or decrease depends on the sign of g_i^j , which is system dependent), whereas the Zeeman splitting requires the knowledge of the Zeeman shifts for each polarization. The total g -factor that modulates the Zeeman splitting is then given by $g_i = g_i^+ - g_i^-$. In pristine monolayer TMDs, $g_X^+ \sim -2$ and $g_X^- \sim 2$ (directly related to the angular momenta of the valence and conduction band states at the K valleys involved in the exciton transition^{53,64}), leading to a total g -factor of $g_X \sim -4$. Furthermore, time reversal symmetry connects the g -factors obtained at positive and negative magnetic fields via $g_i^+(B > 0) = -g_i^-(B < 0)$, allowing us to recover the Zeeman shift of the σ^+ branch by measuring the σ^- branch at negative magnetic

fields.

The excitonic Zeeman shift obtained for the MoSe₂/CrSBr heterostructure is displayed in Figure 3 (d). As a reference, we have also measured the magneto-PL in the MoSe₂/SiO₂ region of the sample [see Figure 3 (e)]. The Zeeman shifts of the trion peaks are presented in Figure S10 and follow closely the excitonic features. Our results reveal an intriguing asymmetric signature in the Zeeman shift of the MoSe₂ exciton within the MoSe₂/CrSBr heterostructure, while the MoSe₂/SiO₂ system displays a symmetric response. These findings point to an asymmetric coupling between the MoSe₂ valleys and the CrSBr bands, which is dependent on the magnetic ordering. Exploiting time reversal symmetry allows us to extract distinct g_i^+ and g_i^- values for each magnetic phase at positive and negative magnetic fields. In Figure 3 (f), we present a schematic representation of the symmetric and asymmetric Zeeman shifts, summarizing the observed features of Figures 3 (d,e). The obtained g -factors for excitons and trions are summarized in Table 1. Particularly, for the excitons in MoSe₂/SiO₂, we extract $|g_{X,T}^+| = |g_{X,T}^-|$ leading to a total g -factor of ~ -4.0 , consistent with theoretical^{53,54,64,65} and experimental values, reported in the literature for MoSe₂/SiO₂ or hBN/MoSe₂/hBN.^{42,45,47,48,52,66-70} For the MoSe₂ excitons on CrSBr, $|g_{X,T}^+|$ is distinctly different from $|g_{X,T}^-|$ and the total g -factor is less negative than the typical values of -4 in pristine MoSe₂. Our study uncovers notable variations in the g -factors of the MoSe₂ exciton and trion when the CrSBr undergoes transitions between the AFM and FM phases, revealing an asymmetric coupling between the spin-valley properties of MoSe₂ and the magnetic ordering of CrSBr. These distinct g -factors provide valuable insights into the intricate interplay between electronic and magnetic degrees of freedom, underscoring the importance of considering the magnetic state of CrSBr in understanding the behavior of excitonic systems in this heterostructure. The changes in the magnitude of the g -factors are consistent with proximity effects due to the hybridization between the layers, as previously demon-

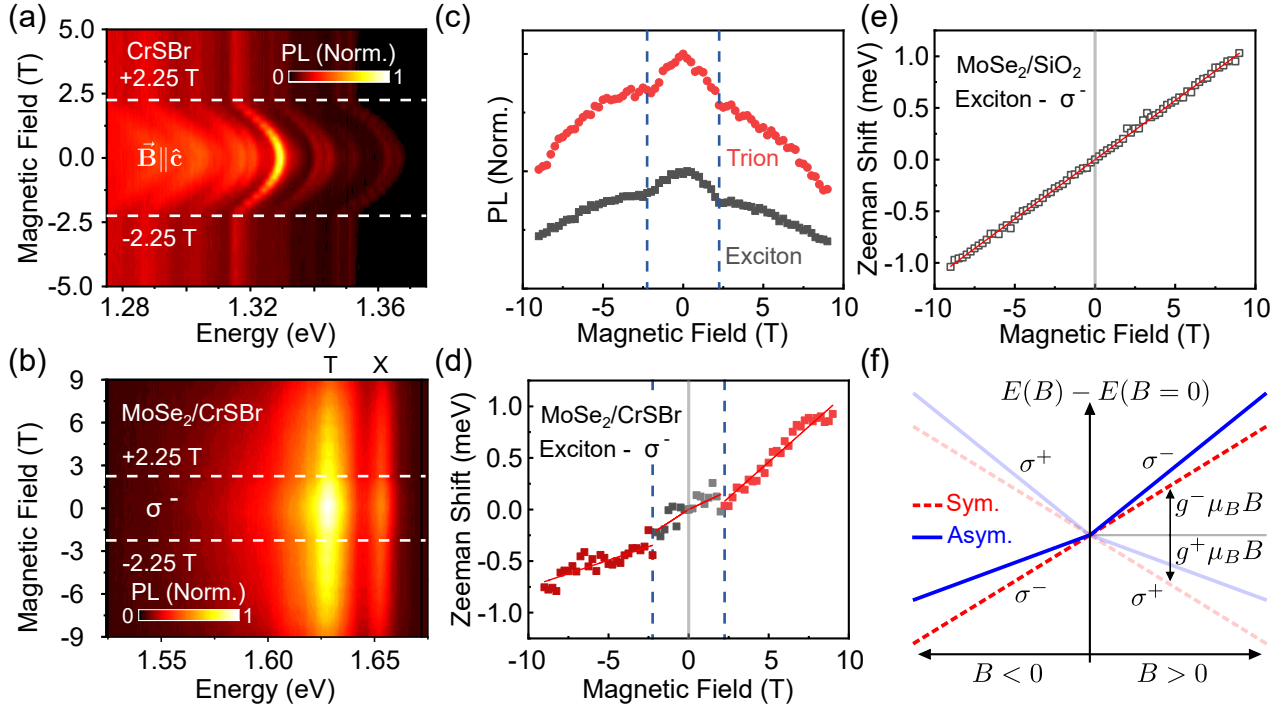


Figure 3: Color-code map of the circularly resolved PL intensity as a function of out-of-plane magnetic field for (a) CrSBr and (b) MoSe₂/CrSBr. The laser excitation is linearly polarized and the PL detection is σ_- for positive magnetic field. (c) PL intensity of exciton and trion peaks of MoSe₂/CrSBr as a function of magnetic field. Zeeman shift for the exciton peaks in the region of (d) MoSe₂/CrSBr and (e) MoSe₂/SiO₂. The solid lines are the fittings to the data. The extracted g -factors are summarized in Table 1. (f) Schematic representation of symmetric (dashed lines) and asymmetric (solid lines) Zeeman shifts as function of magnetic field. The transparent lines indicate the σ^+ polarization that is not being measured.

strated in MoSe₂/WSe₂,^{53,71} WSe₂/CrI₃,⁷² and WS₂/graphene systems.⁷³ A systematic analysis of the microscopic features behind the asymmetric g -factors is beyond the scope of the current manuscript; however, we point out that asymmetric signatures in valley Zeeman splitting have recently been observed in MoSe₂/CrBr₃¹⁶ heterostructures at zero magnetic field. In these systems the magnetic moments in CrBr₃ point in the out-of-plane direction and act already as an external magnetic field. Here, the magnetic moments of CrSBr are oriented in-plane and therefore the asymmetric coupling is manifested once we apply an external magnetic field. The asymmetric Zeeman shifts do not necessarily require a magnetic material but can also be present in systems where valence bands are mixed.⁷⁴

Furthermore, we have also measured the linear polarization of the PL of the het-

erostructure [see Figure S4 (f)]. We find that the angle dependence and relative intensity of the trion/exciton of the MoSe₂ PL are clearly modified as compared to 0 T. The observed anisotropy of the relative intensities of MoSe₂ trion/exciton could be explained by an anisotropic band structure of the heterostructure due to proximity effects.

We now analyze the temperature dependence of the PL data shown in Figure 4. For CrSBr, a blue shift of the PL band is observed with decreasing temperature, which is accompanied by a change in the peak shape around the magnetic phase transition (T_N around 132 K). In addition, at 40 K, sharp peaks appear below 1360 meV, together with a clear enhancement of the PL intensity of the peak at around 1330 meV. A clear correlation between the emission peaks and phase transitions in CrSBr is thus present.

Table 1: Exciton and trion g -factors for $B > 0$. The g -factors for σ^+ were obtained via $g_i^+ = -g_i^-(B < 0)$ and the total g -factor is given by $g_i = g_i^+ - g_i^-$. In the AFM phase, accessed by small fields, the Zeeman shifts approach the spectral resolution of the system, resulting in higher error bars for the obtained values. Nevertheless, the errors are still smaller than the extracted g -factors and allow us to unambiguously identify the asymmetric signatures.

		MoSe ₂ /SiO ₂	MoSe ₂ /CrSBr	
			AFM	FM
Exciton	g_X^+	-1.98 ± 0.05	-1.75 ± 0.39	-0.90 ± 0.05
	g_X^-	1.97 ± 0.05	1.25 ± 0.44	2.37 ± 0.05
	g_X	-4.0 ± 0.1	-3.0 ± 0.8	-3.3 ± 0.1
Trion	g_T^+	-2.10 ± 0.05	-1.33 ± 0.18	-1.42 ± 0.06
	g_T^-	2.14 ± 0.05	2.25 ± 0.46	1.84 ± 0.06
	g_T	-4.2 ± 0.1	-3.6 ± 0.6	-3.3 ± 0.1

Important changes are also observed for the PL of MoSe₂. At higher temperatures ($T_N > 132$ K), the trion binding energy of MoSe₂/CrSBr is much lower than that of MoSe₂/SiO₂, probably due to different dielectric constant values of CrSBr and SiO₂. Remarkably, we find an anomalous temperature dependence of the exciton and trion peak positions for MoSe₂/CrSBr. This is visualized in Figure 4 (d) (see also Figures S11 and S12), where we plot the extracted trion binding energies versus temperature. The MoSe₂/CrSBr trion binding energy increases with decreasing temperature between the magnetic phase transitions, while it stabilizes above T_N and below 40 K. A similar anomaly was observed in the temperature dependence of excitons in the MoSe₂/MnPSe₃ heterostructure near T_N , and was associated to a coupling of MoSe₂ excitons to magnons in MnPSe₃.³ In our heterostructure, MoSe₂ excitons may also couple to the (incoherent) magnons⁵⁷ of CrSBr at non-zero temperatures. The impact of these magnons on the CrSBr band structure has not yet been studied in detail, but it is expected that magnon-induced changes will affect both the charge transfer between MoSe₂ and CrSBr as well as the dielectric screening experienced by the excitons in MoSe₂. Both phenomena may con-

tribute to the exciton/trion temperature dependence.^{75–78} However, further studies will be necessary to understand in more detail this experimental result.

In summary, we have measured the linearly and circularly polarized PL on MoSe₂/CrSBr heterostructures under magnetic fields up to 9 T oriented along the different crystallographic axes of CrSBr. The results show that the valley and excitonic properties (intensity, energy position, and g -factors) of monolayer MoSe₂ are strongly influenced by the magnetic order of a CrSBr substrate. For all magnetic field orientations we found that the MoSe₂ PL intensity is sensitive to the magnetic ordering of the CrSBr. We predict a type-III band alignment for MoSe₂/CrSBr which can account for the observed correlation of MoSe₂ PL intensity with the magnetic induced phase transition of CrSBr. For out-of-plane magnetic fields, a clear asymmetric Zeeman shift is observed for MoSe₂/CrSBr. Furthermore, we observe an anomalous behaviour of the trion binding energy as a function of temperature. The binding energy is considerably low at high temperatures and increases below T_N . In general, our results are explained by asymmetric magnetic proximity, charge transfer, exciton/trion magnon coupling and dielectric anomalies of the 2D anti-

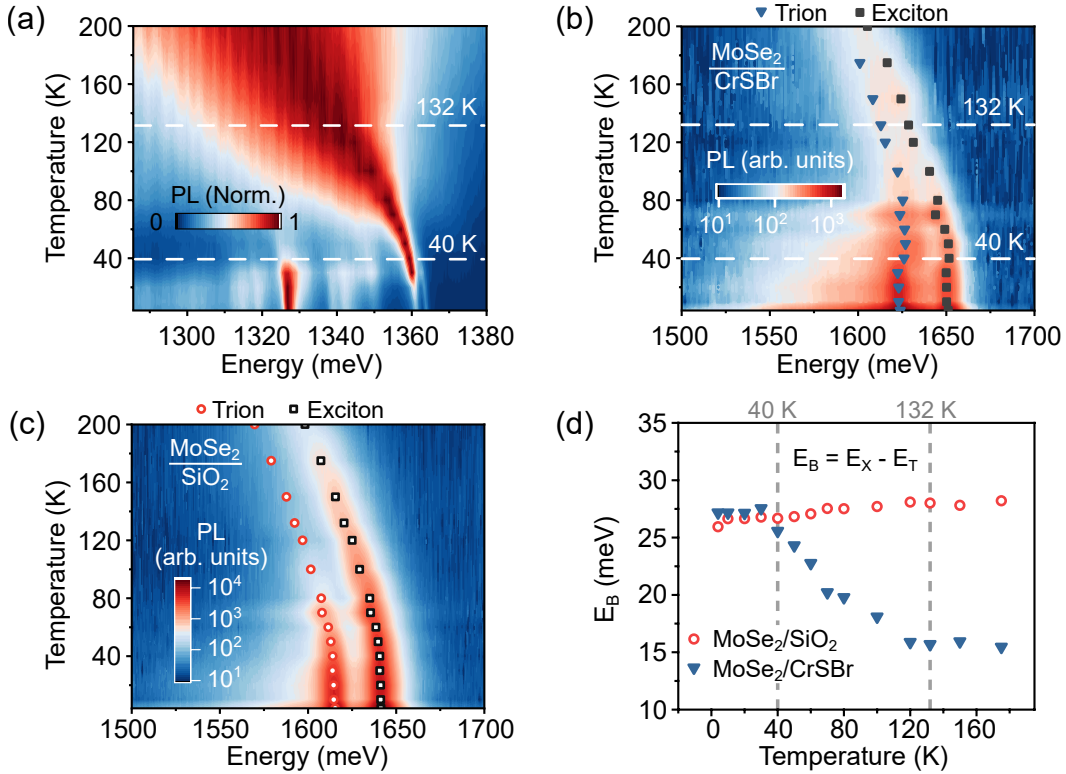


Figure 4: (a) Color-code map of PL intensity as a function of temperature for the PL peaks of the CrSBr. The highest dot-dashed line indicates the CrSBr Néel temperature transition at 132 K, and the lower one at 40 K indicates the temperature where sharpening of the peaks appears. (b,c) Color-code maps of the PL intensity as a function of the temperature for the exciton and trion peaks from (b) MoSe₂/CrSBr and (c) MoSe₂/SiO₂. (d) Trion binding energy extracted from the data shown in (c) and (d).

ferromagnetic material. Our findings offer a unique insight into the interplay of proximity effects and charge transfer in antiferromagnetic-nonmagnetic interfaces that modify the exciton and valley properties of 2D TMDs.

Acknowledgement This work was supported by Fundação de Amparo a Pesquisa do Estado de São Paulo (FAPESP) (grants 22/08329-0 and 23/01313-4) and by the Brazilian Council for Research (CNPq) (grant 311678/2020-3). CSB acknowledges the financial support of CAPES fellowship. TSG and HvdZ received funding from European Union Horizon 2020 research and innovation program under grant agreement No. 863098 (SPRING). PEFJ, KZ, CS, and JF acknowledge the financial support of the Deutsche Forschungsgemeinschaft (DFG, German Research Foundation) SFB 1277 (Project-ID 314695032, projects B05, B07 and B11), SPP 2244 (Project No.

443416183, SCHU1171/10), and of the European Union Horizon 2020 Research and Innovation Program under Contract No. 881603 (Graphene Flagship). YGG and HvdZ acknowledge support from the Fapesp-SPRINT project (grant 22/00419-0). K.W. and T.T. acknowledge support from the JSPS KAKENHI (Grant Numbers 21H05233 and 23H02052) and World Premier International Research Center Initiative (WPI), MEXT, Japan. S.M.-V. acknowledges the European Commission for a Marie Skłodowska–Curie individual fellowship No. 101103355 - SPIN-2D-LIGHT. J.I.A. acknowledges support from the European Union’s Horizon 2020 research and innovation programme for a Marie Skłodowska–Curie individual fellowship No. 101027187-PCSV. F.D. acknowledges financial support from Alexey Chernikov and the Würzburg-Dresden Cluster of Excellence on Complexity and Topology in Quantum Matter

Supporting Information Available

The following files are available free of charge.

- SI: Sample preparation, experimental methods and complementary PL results. Details on the first principles calculations. (PDF)

References

- (1) Lyons, T. P.; Gillard, D.; Molina-Sánchez, A.; Misra, A.; Withers, F.; Keatley, P. S.; Kozikov, A.; Taniguchi, T.; Watanabe, K.; Novoselov, K. S.; Fernández-Rossier, J.; Tartakovskii, A. I. Interplay between spin proximity effect and charge-dependent exciton dynamics in MoSe₂/CrBr₃ van der Waals heterostructures. *Nature Communications* **2020**, *11*, 1–9.
- (2) Zhong, D.; Seyler, K. L.; Linpeng, X.; Wilson, N. P.; Taniguchi, T.; Watanabe, K.; McGuire, M. A.; Fu, K. M. C.; Xiao, D.; Yao, W.; Xu, X. Layer-resolved magnetic proximity effect in van der Waals heterostructures. *Nature Nanotechnology* **2020**, *15*, 187–191.
- (3) Onga, M.; Onga, M.; Sugita, Y.; Ideue, T.; Nakagawa, Y.; Nakagawa, Y.; Suzuki, R.; Suzuki, R.; Motome, Y.; Iwasa, Y.; Iwasa, Y. Antiferromagnet-Semiconductor Van der Waals Heterostructures: Interlayer Interplay of Exciton with Magnetic Ordering. *Nano Letters* **2020**, *20*, 4625–4630.
- (4) Li, Y.; Yang, B.; Xu, S.; Huang, B.; Duan, W. Emergent Phenomena in Magnetic Two-Dimensional Materials and van der Waals Heterostructures. *ACS Applied Electronic Materials* **2022**, *4*, 3278–3302.
- (5) Choi, E.-M.; Sim, K. I.; Burch, K. S.; Lee, Y. H.; Choi, E.-M.; Sim, K. I.; Lee, Y. H.; Burch, K. S. Emergent Multifunctional Magnetic Proximity in van der Waals Layered Heterostructures. *Advanced Science* **2022**, *9*, 2200186.
- (6) Seyler, K. L.; Zhong, D.; Huang, B.; Linpeng, X.; Wilson, N. P.; Taniguchi, T.; Watanabe, K.; Yao, W.; Xiao, D.; McGuire, M. A.; Fu, K. M. C.; Xu, X. Valley Manipulation by Optically Tuning the Magnetic Proximity Effect in WSe₂/CrI₃ Heterostructures. *Nano Letters* **2018**, *18*, 3823–3828.
- (7) Pawbake, A. et al. Magneto-optical sensing of the pressure driven magnetic ground states in bulk CrSBr. *arXiv preprint arXiv:2303.01823* **2023**,
- (8) Scharf, B.; Xu, G.; Matos-Abiague, A.; Žutić, I. Magnetic Proximity Effects in Transition-Metal Dichalcogenides: Converting Excitons. *Physical Review Letters* **2017**, *119*, 127403.
- (9) Huang, B.; Clark, G.; Navarro-Moratalla, E.; Klein, D. R.; Cheng, R.; Seyler, K. L.; Zhong, D.; Schmidgall, E.; McGuire, M. A.; Cobden, D. H.; Yao, W.; Xiao, D.; Jarillo-Herrero, P.; Xu, X. Layer-dependent ferromagnetism in a van der Waals crystal down to the monolayer limit. *Nature* **2017**, *546*, 270–273.
- (10) Zhang, Z.; Ni, X.; Huang, H.; Hu, L.; Liu, F. Valley splitting in the van der Waals heterostructure WSe₂/CrI₃: The role of atom superposition. *Physical Review B* **2019**, *99*, 115441.
- (11) Xie, J.; Jia, L.; Shi, H.; Yang, D.; Si, M. Electric field mediated large valley splitting in the van der Waals heterostructure WSe₂/CrI₃. *Japanese Journal of Applied Physics* **2018**, *58*, 010906.
- (12) Ahn, E. C. 2D materials for spintronic devices. *npj 2D Materials and Applications* **2020** *4:1* **2020**, *4*, 1–14.

- (13) Boix-Constant, C. et al. Probing the Spin Dimensionality in Single-Layer CrSBr Van Der Waals Heterostructures by Magneto-Transport Measurements. *Advanced Materials* **2022**, *34*, 2204940.
- (14) Geim, A. K.; Grigorieva, I. V. Van der Waals heterostructures. *Nature* **2013**, *499*, 419–425.
- (15) Novoselov, K. S.; Mishchenko, A.; Carvalho, A.; Neto, A. H. C. 2D materials and van der Waals heterostructures. *Science* **2016**, *353*.
- (16) Choi, J.; Lane, C.; Zhu, J. X.; Crooker, S. A. Asymmetric magnetic proximity interactions in MoSe₂/CrBr₃ van der Waals heterostructures. *Nature Materials* **2022**, *22*, 305–310.
- (17) Zhong, D.; Seyler, K. L.; Linpeng, X.; Cheng, R.; Sivadas, N.; Huang, B.; Schmidgall, E.; Taniguchi, T.; Watanabe, K.; McGuire, M. A.; Yao, W.; Xiao, D.; Fu, K. M. C.; Xu, X. Van der Waals engineering of ferromagnetic semiconductor heterostructures for spin and valleytronics. *Science Advances* **2017**, *3*.
- (18) Huang, B.; McGuire, M. A.; May, A. F.; Xiao, D.; Jarillo-Herrero, P.; Xu, X. Emergent phenomena and proximity effects in two-dimensional magnets and heterostructures. *Nature Materials* **2020**, *19*, 1276–1289.
- (19) Mak, K. F.; Shan, J.; Ralph, D. C. Probing and controlling magnetic states in 2D layered magnetic materials. *Nature Reviews Physics* **2019**, *1*, 646–661.
- (20) Zollner, K.; Faria Junior, P. E.; Fabian, J. Proximity exchange effects in MoSe₂ and WSe₂ heterostructures with CrI₃: Twist angle, layer, and gate dependence. *Physical Review B* **2019**, *100*.
- (21) Zollner, K.; Faria Junior, P. E.; Fabian, J. Giant proximity exchange and valley splitting in transition metal dichalcogenide/hBN/(Co, Ni) heterostructures. *Phys. Rev. B* **2020**, *101*, 085112.
- (22) Zollner, K.; Faria Junior, P. E.; Fabian, J. Strong manipulation of the valley splitting upon twisting and gating in MoSe₂/CrI₃ and WSe₂/CrI₃ van der Waals heterostructures. *Phys. Rev. B* **2023**, *107*, 035112.
- (23) Zhao, C. et al. Enhanced valley splitting in monolayer WSe₂ due to magnetic exchange field. *Nature Nanotechnology* **2017**, *12*, 757–762.
- (24) Norden, T.; Zhao, C.; Zhang, P.; Sabirianov, R.; Petrou, A.; Zeng, H. Giant valley splitting in monolayer WS₂ by magnetic proximity effect. *Nature Communications* **2019**, *10*, 1–10.
- (25) Ciorciaro, L.; Kroner, M.; Watanabe, K.; Taniguchi, T.; Imamoglu, A. Observation of Magnetic Proximity Effect Using Resonant Optical Spectroscopy of an Electrically Tunable MoSe₂/CrBr₃ Heterostructure. *Physical Review Letters* **2020**, *124*, 197401.
- (26) Klein, J. et al. Sensing the Local Magnetic Environment through Optically Active Defects in a Layered Magnetic Semiconductor. *ACS Nano* **2023**, *17*, 288–299.
- (27) Lee, K.; Dismukes, A. H.; Telford, E. J.; Wiscons, R. A.; Wang, J.; Xu, X.; Nuckolls, C.; Dean, C. R.; Roy, X.; Zhu, X. Magnetic Order and Symmetry in the 2D Semiconductor CrSBr. *Nano Letters* **2021**, *21*, 3511–3517.
- (28) Wilson, N. P.; Lee, K.; Cenker, J.; Xie, K.; Dismukes, A. H.; Telford, E. J.; Fonseca, J.; Sivakumar, S.; Dean, C.; Cao, T.; Roy, X.; Xu, X.; Zhu, X. Interlayer electronic coupling on demand in a 2D magnetic semiconductor. *Nature Materials* **2021**, *20*, 1657–1662.
- (29) Telford, E. J. et al. Coupling between magnetic order and charge transport in a

- two-dimensional magnetic semiconductor. *Nature Materials* **2022**, *21*, 754–760.
- (30) López-Paz, S. A.; Guguchia, Z.; Pomjakushin, V. Y.; Witteveen, C.; Cervellino, A.; Luetkens, H.; Casati, N.; Morpurgo, A. F.; von Rohr, F. O. Dynamic magnetic crossover at the origin of the hidden-order in van der Waals antiferromagnet CrSBr. *Nature Communications* **2022**, *13*, 1–10.
- (31) Ye, C.; Wang, C.; Wu, Q.; Liu, S.; Zhou, J.; Wang, G.; Söll, A.; Sofer, Z.; Yue, M.; Liu, X.; Tian, M.; Xiong, Q.; Ji, W.; Wang, X. R. Layer-Dependent Interlayer Antiferromagnetic Spin Reorientation in Air-Stable Semiconductor CrSBr. *ACS Nano* **2022**, *16*, 11876–11883.
- (32) Ghiasi, T. S.; Kaverzin, A. A.; Dismukes, A. H.; de Wal, D. K.; Roy, X.; van Wees, B. J. Electrical and thermal generation of spin currents by magnetic bilayer graphene. *Nature Nanotechnology* **2021**, *16*, 788–794.
- (33) Bae, Y. J. et al. Exciton-coupled coherent magnons in a 2D semiconductor. *Nature* **2022**, *609*, 282–286.
- (34) Klein, J. et al. The Bulk van der Waals Layered Magnet CrSBr is a Quasi-1D Material. *ACS Nano* **2023**,
- (35) Mak, K. F.; Lee, C.; Hone, J.; Shan, J.; Heinz, T. F. Atomically thin MoS₂: A new direct-gap semiconductor. *Physical Review Letters* **2010**, *105*, 136805.
- (36) Splendiani, A.; Sun, L.; Zhang, Y.; Li, T.; Kim, J.; Chim, C. Y.; Galli, G.; Wang, F. Emerging photoluminescence in monolayer MoS₂. *Nano Letters* **2010**, *10*, 1271–1275.
- (37) Xu, X.; Yao, W.; Xiao, D.; Heinz, T. F. Spin and pseudospins in layered transition metal dichalcogenides. *Nature Physics* **2014**, *10*, 343–350.
- (38) Xiao, D.; Liu, G. B.; Feng, W.; Xu, X.; Yao, W. Coupled spin and valley physics in monolayers of MoS₂ and other group-VI dichalcogenides. *Physical Review Letters* **2012**, *108*, 196802.
- (39) Mak, K. F.; He, K.; Shan, J.; Heinz, T. F. Control of valley polarization in monolayer MoS₂ by optical helicity. *Nature Nanotechnology* **2012**, *7*, 494–498.
- (40) Zeng, H.; Dai, J.; Yao, W.; Xiao, D.; Cui, X. Valley polarization in MoS₂ monolayers by optical pumping. *Nature Nanotechnology* **2012**, *7*, 490–493.
- (41) Schaibley, J. R.; Yu, H.; Clark, G.; Rivera, P.; Ross, J. S.; Seyler, K. L.; Yao, W.; Xu, X. Valleytronics in 2D materials. *Nature Reviews Materials* **2016**, *1*, 1–15.
- (42) Gobato, Y. G.; Brito, C. S. D.; Chaves, A.; Prosnikov, M. A.; Woźniak, T.; Guo, S.; Barcelos, I. D.; Milošević, M. V.; Withers, F.; Christianen, P. C. Distinctive g-Factor of Moiré-Confined Excitons in van der Waals Heterostructures. *Nano Letters* **2022**, *22*, 8641–8646.
- (43) Ishii, S.; Yokoshi, N.; Ishihara, H. Optical selection rule of monolayer transition metal dichalcogenide by an optical vortex. *Journal of Physics: Conference Series* **2019**, *1220*, 012056.
- (44) Aivazian, G.; Gong, Z.; Jones, A. M.; Chu, R. L.; Yan, J.; Mandrus, D. G.; Zhang, C.; Cobden, D.; Yao, W.; Xu, X. Magnetic control of valley pseudospin in monolayer WSe₂. *Nature Physics* **2015**, *11*, 148–152.
- (45) Li, Y.; Ludwig, J.; Low, T.; Chernikov, A.; Cui, X.; Arefe, G.; Kim, Y. D.; Zande, A. M. V. D.; Rigosi, A.; Hill, H. M.; Kim, S. H.; Hone, J.; Li, Z.; Smirnov, D.; Heinz, T. F. Valley splitting and polarization by the zeeman effect in monolayer MoSe₂. *Physical Review Letters* **2014**, *113*, 266804.

- (46) Srivastava, A.; Sidler, M.; Allain, A. V.; Lembke, D. S.; Kis, A.; Imamoglu, A. Valley Zeeman effect in elementary optical excitations of monolayer WSe₂. *Nature Physics* **2015**, *11*, 141–147.
- (47) Macneill, D.; Heikes, C.; Mak, K. F.; Anderson, Z.; Kormányos, A.; Zólyomi, V.; Park, J.; Ralph, D. C. Breaking of valley degeneracy by magnetic field in monolayer MoSe₂. *Physical Review Letters* **2015**, *114*, 037401.
- (48) Wang, G.; Bouet, L.; Glazov, M. M.; Amand, T.; Ivchenko, E. L.; Palleau, E.; Marie, X.; Urbaszek, B. Magneto-optics in transition metal diselenide monolayers. *2D Materials* **2015**, *2*, 034002.
- (49) Mitioglu, A. A.; Plochocka, P.; Aguila, G. D.; Christianen, P. C.; Deligeorgis, G.; Anghel, S.; Kulyuk, L.; Maude, D. K. Optical Investigation of Monolayer and Bulk Tungsten Diselenide (WSe₂) in High Magnetic Fields. *Nano Letters* **2015**, *15*, 4387–4392.
- (50) Stier, A. V.; McCreary, K. M.; Jonker, B. T.; Kono, J.; Crooker, S. A. Exciton diamagnetic shifts and valley Zeeman effects in monolayer WS₂ and MoS₂ to 65 Tesla. *Nature Communications* **2016**, *7*, 1–8.
- (51) Plechinger, G.; Nagler, P.; Arora, A.; Águila, A. G. D.; Ballottin, M. V.; Frank, T.; Steinleitner, P.; Gmitra, M.; Fabian, J.; Christianen, P. C.; Bratschitsch, R.; Schüller, C.; Korn, T. Excitonic Valley Effects in Monolayer WS₂ under High Magnetic Fields. *Nano Letters* **2016**, *16*, 7899–7904.
- (52) Covre, F. S.; Faria Junior, P. E.; Gordo, V. O.; de Brito, C. S.; Zhumagulov, Y. V.; Teodoro, M. D.; Couto, O. D.; Misoguti, L.; Pratavieira, S.; Andrade, M. B.; Christianen, P. C.; Fabian, J.; Withers, F.; Gobato, Y. G. Revealing the impact of strain in the optical properties of bubbles in monolayer MoSe₂. *Nanoscale* **2022**, *14*, 5758–5768.
- (53) Woźniak, T.; Faria Junior, P. E.; Seifert, G.; Chaves, A.; Kunstmann, J. Exciton g factors of van der Waals heterostructures from first-principles calculations. *Physical Review B* **2020**, *101*, 235408.
- (54) Deilmann, T.; Krüger, P.; Rohlfing, M. Ab Initio Studies of Exciton g Factors: Monolayer Transition Metal Dichalcogenides in Magnetic Fields. *Physical Review Letters* **2020**, *124*, 226402.
- (55) Xuan, F.; Quek, S. Y. Valley-filling instability and critical magnetic field for interaction-enhanced Zeeman response in doped WSe₂ monolayers. *npj Computational Materials* **2021**, *7*, 198.
- (56) Back, P.; Sidler, M.; Cotlet, O.; Srivastava, A.; Takemura, N.; Kroner, M.; Imamoğlu, A. Giant Paramagnetism-Induced Valley Polarization of Electrons in Charge-Tunable Monolayer MoSe₂. *Physical Review Letters* **2017**, *118*, 237404.
- (57) Dirnberger, F.; Quan, J.; Bushati, R.; Diederich, G. M.; Florian, M.; Klein, J.; Mosina, K.; Sofer, Z.; Xu, X.; Kamra, A.; García-Vidal, F. J.; Alù, A.; Menon, V. M. Magneto-optics in a van der Waals magnet tuned by self-hybridized polaritons. *Nature* **2023**, *620*:7974, *620*, 533–537.
- (58) Marques-Moros, F.; Boix-Constant, C.; Mañas-Valero, S.; Canet-Ferrer, J.; Coronado, E. Interplay between Optical Emission and Magnetism in the van der Waals Magnetic Semiconductor CrSBr in the Two-Dimensional Limit. *ACS Nano* **2023**, *17*, 13224–13231.
- (59) Lin, K.; Sun, X.; Dirnberger, F.; Li, Y.; Qu, J.; Wen, P.; Sofer, Z.; Söll, A.; Winnerl, S.; Helm, M.; Zhou, S.; Dan, Y.;

- Prucnal, S. Strong Exciton-Phonon Coupling as a Fingerprint of Magnetic Ordering in van der Waals Layered CrSBr. *arXiv preprint arXiv:2308.04895* **2023**,
- (60) Schwemmer, M.; Nagler, P.; Hanning, A.; Schüller, C.; Korn, T. Long-lived spin polarization in n-doped MoSe₂ monolayers. *Appl. Phys. Lett.* **2017**, *111*.
- (61) Bianchi, M.; Acharya, S.; Dirnberger, F.; Klein, J.; Pashov, D.; Mosina, K.; Sofer, Z.; Rudenko, A. N.; Katsnelson, M. I.; van Schilfgaarde, M.; Röchner, M.; Hofmann, P. Paramagnetic electronic structure of CrSBr: Comparison between ab initio GW theory and angle-resolved photoemission spectroscopy. *Physical Review B* **2023**, *107*.
- (62) Stier, A. V.; Wilson, N. P.; Velizhanin, K. A.; Kono, J.; Xu, X.; Crooker, S. A. Magneto-optics of Exciton Rydberg States in a Monolayer Semiconductor. *Phys. Rev. Lett.* **2018**, *120*, 057405.
- (63) Klein, J.; Hötger, A.; Florian, M.; Steinhoff, A.; Delhomme, A.; Taniguchi, T.; Watanabe, K.; Jahnke, F.; Holleitner, A. W.; Potemski, M.; Faugeras, C.; Finley, J. J.; Stier, A. V. Controlling exciton many-body states by the electric-field effect in monolayer MoS₂. *Phys. Rev. Res.* **2021**, *3*, L022009.
- (64) Faria Junior, P. E.; Zollner, K.; Woźniak, T.; Kurpas, M.; Gmitra, M.; Fabian, J. First-principles insights into the spin-valley physics of strained transition metal dichalcogenides monolayers. *New Journal of Physics* **2022**, *24*, 083004.
- (65) Xuan, F.; Quek, S. Y. Valley Zeeman effect and Landau levels in two-dimensional transition metal dichalcogenides. *Physical Review Research* **2020**, *2*, 033256.
- (66) Mitiglu, A. A.; Galkowski, K.; Surrente, A.; Klopotoski, L.; Dumcenco, D.; Kis, A.; Maude, D. K.; Plochocka, P. Magnetoexcitons in large area CVD-grown monolayer MoS₂ and MoSe₂ on sapphire. *Physical Review B* **2016**, *93*, 165412.
- (67) Arora, A.; Koperski, M.; Slobodeniuk, A.; Nogajewski, K.; Schmidt, R.; Schneider, R.; Molas, M. R.; Vasconcellos, S. M. D.; Bratschitsch, R.; Potemski, M. Zeeman spectroscopy of excitons and hybridization of electronic states in few-layer WSe₂, MoSe₂ and MoTe₂. *2D Materials* **2018**, *6*, 015010.
- (68) Koperski, M.; Molas, M. R.; Arora, A.; Nogajewski, K.; Bartos, M.; Wyzula, J.; Vaclavkova, D.; Kossacki, P.; Potemski, M. Orbital, spin and valley contributions to Zeeman splitting of excitonic resonances in MoSe₂, WSe₂ and WS₂ Monolayers. *2D Materials* **2018**, *6*, 015001.
- (69) Goryca, M.; Li, J.; Stier, A. V.; Taniguchi, T.; Watanabe, K.; Courtade, E.; Shree, S.; Robert, C.; Urbaszek, B.; Marie, X.; Crooker, S. A. Revealing exciton masses and dielectric properties of monolayer semiconductors with high magnetic fields. *Nature Communications* **2019** *10:1* **2019**, *10*, 1–12.
- (70) Robert, C.; Han, B.; Kapuscinski, P.; Delhomme, A.; Faugeras, C.; Amand, T.; Molas, M. R.; Bartos, M.; Watanabe, K.; Taniguchi, T.; Urbaszek, B.; Potemski, M.; Marie, X. Measurement of the spin-forbidden dark excitons in MoS₂ and MoSe₂ monolayers. *Nature Communications* **2020** *11:1* **2020**, *11*, 1–8.
- (71) Faria Junior, P. E.; Fabian, J. Signatures of Electric Field and Layer Separation Effects on the Spin-Valley Physics of MoSe₂/WSe₂ Heterobilayers: From Energy Bands to Dipolar Excitons. *Nanomaterials* **2023**, *13*.
- (72) Heißenbüttel, M.-C.; Deilmann, T.; Krüger, P.; Rohlffing, M. Valley-Dependent Interlayer Excitons in

Magnetic WSe₂/CrI₃. *Nano Letters* **2021**, *21*, 5173.

- (73) Faria Junior, P. E.; Naimer, T.; McCreary, K. M.; Jonker, B. T.; Finley, J. J.; Crooker, S. A.; Fabian, J.; Stier, A. V. Proximity-enhanced valley Zeeman splitting at the WS₂/graphene interface. *2D Materials* **2023**, *10*, 034002.
- (74) Tedeschi, D.; De Luca, M.; Faria Junior, P. E.; Granados del Águila, A.; Gao, Q.; Tan, H. H.; Scharf, B.; Christensen, P. C. M.; Jagadish, C.; Fabian, J.; Polimeni, A. Unusual spin properties of InP wurtzite nanowires revealed by Zeeman splitting spectroscopy. *Phys. Rev. B* **2019**, *99*, 161204.
- (75) Tuan, D. V.; Yang, M.; Dery, H. Coulomb interaction in monolayer transition-metal dichalcogenides. *Physical Review B* **2018**, *98*, 125308.
- (76) Florian, M.; Hartmann, M.; Steinhoff, A.; Klein, J.; Holleitner, A. W.; Finley, J. J.; Wehling, T. O.; Kaniber, M.; Gies, C. The Dielectric Impact of Layer Distances on Exciton and Trion Binding Energies in van der Waals Heterostructures. *Nano Letters* **2018**, *18*, 2725–2732.
- (77) Zhumagulov, Y. V.; Vagov, A.; Senkevich, N. Y.; Gulevich, D. R.; Perebeinos, V. Three-particle states and brightening of intervalley excitons in a doped MoS₂ monolayer. *Physical Review B* **2020**, *101*, 245433.
- (78) Lin, Y.; Ling, X.; Yu, L.; Huang, S.; Hsu, A. L.; Lee, Y. H.; Kong, J.; Dresselhaus, M. S.; Palacios, T. Dielectric screening of excitons and trions in single-layer MoS₂. *Nano Letters* **2014**, *14*, 5569–5576.